



Free vibration of functionally graded viscoelastic foam plates using shear- and normal-deformation theories

H.A. Zamani¹

Received: 3 August 2021 / Accepted: 7 December 2021 / Published online: 30 January 2022
© The Author(s), under exclusive licence to Springer Nature B.V. 2021

Abstract

In this paper, various shear- and normal-deformation theories with polynomial, hyperbolic and integral functions of displacements are applied to examine thickness-stretching effects on the free vibration of thick open-cell foam plates. Displacement functions include bending, shear and thickness stretching of transverse deflection. The distribution of porosity through the thickness is considered by a power-law relationship, while the separable kernel framework and Boltzmann–Volterra superposition principles are used to describe the constitutive relations. Also, a standard solid viscoelastic model is investigated as a special case. The integropartial differential equations of motion with frequency-dependent coefficients based on different deformation theories are derived using the Hamilton principle in the complex domain, and they are solved via semianalytical and iterative numerical algorithms in the spatial and frequency domains. The solution procedure is assessed for elastic functionally graded plates and viscoelastic laminated plates. The effects of porosity distribution, thickness stretching, different deformation theories and geometrical parameters on natural frequencies and loss factors are investigated through parametric studies and it is revealed that the results obtained from deformation theories with integral functions give the nearest loss factors to the layerwise theory, the highest vibrational characteristics and are most affected by the power index in comparison with other theories.

Keywords Functionally graded materials · Thickness-stretching effect · Shear and normal deformation theory · Semianalytical solution · Open-cell foam

1 Introduction

The time and frequency dependency of functionally graded (FG) materials play a key role in the analysis and design of plates in various fields like aerospace, mechanical, biomechanics to name but a few (Altenbach and Eremeyev 2008a,b,c). Functionally graded polymers or foams may display time/frequency-dependent behavior under normal conditions, complex loading circumstances or extreme thermal environments; however, the mentioned

✉ H.A. Zamani
zamani.h.a@aut.ac.ir

¹ Mechanical Engineering Department, Amirkabir University of Technology (Tehran Polytechnic), 424 Hafez Ave., Tehran, 15875-4413, Iran

behavior, which is known as viscoelastic behavior (Brinson and Brinson 2008), may be justified for FG viscoelastic (FGV) materials. Also, foams such as cellular materials may be divided into closed-cell or no interconnected networks and open-cell or interconnected networks (Ashby et al. 2000; Miracle et al. 2001; Taraz Jamshidi et al. 2015; Hedayati and Sadighi 2016; Sadeghnejad et al. 2017). These foams, due to significant characteristics such as low weight, high specific strength and inherent damping have attracted great attention (Altenbach and Eremeyev 2009; Al Jahwari et al. 2016; Montgomery et al. 2021). It should be noted that FGV foam plates have the merits of FG and viscoelastic plates simultaneously. In fact, addition of the viscoelastic property to FG plates could enhance energy dissipation, noise reduction and vibrational damping of FG plates that are used in various industries, as mentioned previously. Moreover, FGV plates could be produced via adding a constrained viscoelastic layer on the surfaces of FG materials or production of viscoelastic foams in a specific manner. Hence, FGV plates may be considered as a candidate for FG plates that face dynamic loads or viscoelastic foam plates, which demand graded properties.

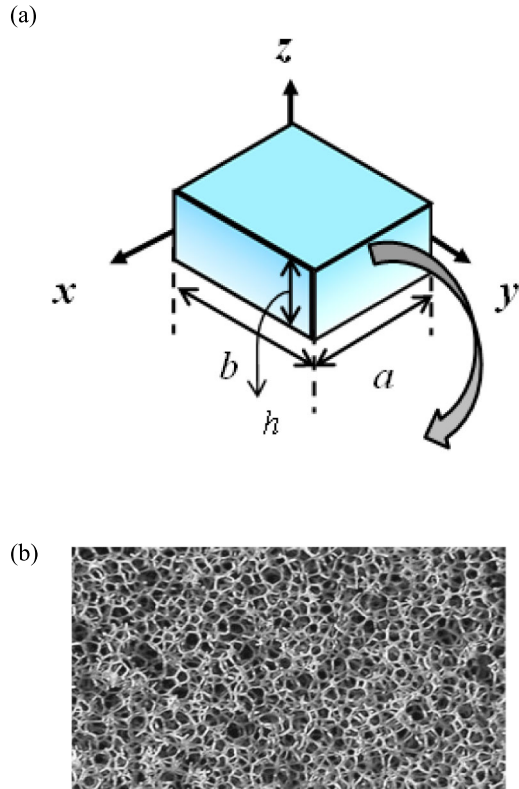
Although viscoelastic behavior is mainly observed for polymeric matrix or composites with polymeric elements, some studies considered viscoelastic behavior of whole FG plates via a simple differentiation operator of the Kelvin–Voigt model. Gupta and Kumar (2008) considered classical plate theory (CPT) and Levy-type boundary conditions of rectangular plates with variable thickness, longitudinal nonhomogeneity and linear temperature/spatial-dependent moduli. Their results demonstrated that nonhomogeneous plates have lower time period and logarithmic decrement than homogeneous plates. Sofiyev et al. (2019) studied dynamic buckling of simply supported plates on an elastic foundation using the Galerkin method, Laplace transform and CPT. Hilton and Lee (2012) applied the Galerkin method and generalized Kelvin model to derive long-term responses of simply supported plates under simultaneous aerodynamic, creep, thermal, magnetic and electric loads. Shariyat and Farzan Nasab (2014) applied the standard solid model, the Mori–Tanaka micromechanical approach, a modified Hertz law, refined higher-order shear deformation theory (RHSDT) and the differential quadrature method to study low-velocity impact responses of plates. They concluded that the viscoelasticity of materials has a significant influence on the dynamic responses of plates after impact. Shariyat and Farrokhi (2019) extended the previous study for the transient and forced vibrations of microplates via CPT, the Navier solution and Runge–Kutta integration methods. Zhang and coauthors (Zhang and Wang 2006; Zhang and Xing 2008) presented transient responses of thin FGV plates based on the Boltzmann superposition integral and the Legendre–Ritz method. Zamani et al. (2018) used a physical neutral surface, CPT, the Boltzmann–Volterra superposition integral and the Galerkin method to achieve frequencies of open-cell foam plates resting on an orthotropic visco-Pasternak medium under various boundary conditions. It is worth noting that the Boltzmann–Volterra superposition integral is more suitable than the differential operator in the complex domain. Recently, Shariyat and Jahangiri (2020) applied a 3-dimensional Zener viscoelastic model, nonlinear Hertz law and finite-element method to achieve impact responses of partially supported porous viscoelastic plates under bending-induced fluid-flow loads. Furthermore, from the practical and theoretical points of view, thick and very thick FG and laminated composite plates have significant impact and numerous applications, therefore, to achieve an accurate analysis, both shear and normal deformations should be considered in kinematic relations (Carrera et al. 2011). Fortunately, higher-order shear and normal deformation theory (HSNDT) may meet the required accuracy and functionality (Thai et al. 2020b; Thai and Phung-Van 2020; Phung-Van and Thai 2021; Phung-Van et al. 2021; Jafari and Kiani 2021), whereas the considered studies of FGV plates place an emphasis on

CPT and RHSD, which neglect shear and normal deformations in the thickness direction, respectively.

Higher-order shear and normal deformation theories consider transverse normal strain or the thickness-stretching effect, which has inevitable roles in the reliable and accurate kinematic relations of thick and moderately thick FG plates and shells (Carrera et al. 2011). As mentioned, applications of HSNDTs of FGV plates have received less attention from researchers, although there are numerous investigations on applications of HSDT and HSNDT for FG elastic plates (Thai et al. 2013, 2016a,b, 2020a). Indeed, the thickness-stretching effect could be applied through the governing equations of motion considering normal strain in the thickness direction. This strain extends the number of unknown variables in the displacement field and kinematic relations and eventually it provides some complexity to solve the coupled governing equations of motion (Carrera et al. 2011). This remark may be modified by separation of transverse displacement into shear, bending, thickness-stretching parts and the implementation of stress-free boundary conditions on the top and bottom surfaces of the plate. Therefore, the total number of unknowns remains at four or five regarding the assumed elements of displacement fields. Among the presented theories, one may refer to five unknowns HSNDT with polynomial functions (HSNDT-Poly) (Thai and Choi 2014), HSNDT with hyperbolic functions (HSNDT-Hyp) (Belabed et al. 2014), quasithree-dimensional with trigonometric functions (Quasi-3D-Tri) (Abualnour et al. 2018), Quasi-3D with integral variables (Quasi-3D-Int) (Zaoui et al. 2019). Also, there are six to nine unknown theories such as Quasi-3D sinusoidal shear deformation theory (Quasi-3D-SSDT) (Neves et al. 2012b), Quasi-3D hyperbolic shear deformation theory (Quasi-3D-HYP) (Neves et al. 2012a) and Quasi-3D HSDT (Neves et al. 2013). Recently, Karamanli and Aydogdu (2020) used the HSNDT, finite-element method and modified coupled stress theory to obtain the frequencies of porous microplates. For completeness, one may refer to other papers that investigated vibrations of FG elastic plates and beams with thickness-stretching effect, see for instance (Meksi et al. 2015; Allam et al. 2020; Bendenia et al. 2020; Menasria et al. 2020; Tahir et al. 2021a,b; Zaitoun et al. 2021). Obviously, the main concentration of the mentioned theories is located on the thickness stretching of FG elastic plates whereas the application of thickness-stretching effects on the dynamics of FGV foam plates appears to be missing from the literature.

Based on a literature survey, it is observed that the investigations of free vibration of FGV plates are merely assigned to plates with CPT (Zhang and Wang 2006; Zhang and Xing 2008; Gupta and Kumar 2008; Hilton and Lee 2012; Zamani et al. 2018; Sofiyev et al. 2019; Shariyat and Farrokhi 2019), RHSDT (Shariyat and Farzan Nasab 2014) and 3D theory (Shariyat and Jahangiri 2020). In addition, the effects of thickness stretching on the vibrations of FG plates are only taken into account in the elastic domain (Thai et al. 2020b; Thai and Phung-Van 2020; Phung-Van and Thai 2021; Phung-Van et al. 2021; Jafari and Kiani 2021; Thai et al. 2013, 2016a,b, 2020a; Carrera et al. 2011; Thai and Choi 2014; Belabed et al. 2014; Abualnour et al. 2018; Zaoui et al. 2019; Neves et al. 2012b; Neves et al. 2012a, 2013; Karamanli and Aydogdu 2020; Tahir et al. 2021a,b; Zaitoun et al. 2021). Furthermore, viscoelastic behaviors of FGV plates are generally simulated via a simple differential operator, while the application of the Boltzmann–Volterra superposition integral of vibrations of FGV plates is limited to classical (Zamani et al. 2018) and 3D (Shariyat and Jahangiri 2020) plate theories. Therefore, there is no study on the vibrations of FGV foam plates considering thickness-stretching effects via polynomial, hyperbolic, integral displacement functions and Boltzmann–Volterra superposition principles of the viscoelastic model.

Fig. 1 The geometry and coordinates of a functionally graded viscoelastic plate **(a)**, schematic of a polymeric open-cell foam **(b)** (Altenbach and Eremeyev 2008c)



In this study, the impacts of thickness stretching on the vibrational characteristics of simply supported viscoelastic foam plates with FG distributions of properties are investigated. The Boltzmann–Volterra superposition integral, separable kernels and three different displacement fields are applied to establish constitutive and kinematic relations, respectively. The five-coupled integropartial differential equations (PDEs) of motion based on polynomial, hyperbolic and integral displacement functions are derived using the Hamilton principle. The Galerkin method and iterative eigenvalue solver are implemented in the spatial and frequency domains, respectively. The present method is verified for both FG elastic and viscoelastic composite plates. The effects of aspect ratio, thickness parameter, power index, kinematic model and higher modes on natural frequency and modal loss factor are investigated by parametric studies.

2 Basic formulation

Consider a rectangular FGV foam plate as illustrated in Fig. 1. Parameters a , b and h denote length, width and thickness, respectively. Also, the origin point of the Cartesian coordinate system is located at the corner of the midsurface of the plate.

2.1 Constitutive relations

In this paper, the linear viscoelastic behavior of an open-cell foam plate is assumed based on the Boltzmann–Volterra superposition integral as (Brinson and Brinson 2008):

$$\begin{Bmatrix} \sigma_{xx} \\ \sigma_{yy} \\ \sigma_{zz} \\ \sigma_{yz} \\ \sigma_{xz} \\ \sigma_{xy} \end{Bmatrix} = \int_{-\infty}^t \begin{bmatrix} \lambda_1(t-t') & \lambda(t-t') & \lambda(t-t') & 0 & 0 & 0 \\ & \lambda_1(t-t') & \lambda(t-t') & 0 & 0 & 0 \\ & & \lambda_1(t-t') & 0 & 0 & 0 \\ & & & \mu(t-t') & 0 & 0 \\ & & & & \mu(t-t') & 0 \\ & & & & & \mu(t-t') \end{bmatrix} \times \begin{Bmatrix} \varepsilon_{x,t'}(t') \\ \varepsilon_{y,t'}(t') \\ \varepsilon_{z,t'}(t') \\ \varepsilon_{yz,t'}(t') \\ \varepsilon_{xz,t'}(t') \\ \varepsilon_{xy,t'}(t') \end{Bmatrix} dt' \tag{1}$$

where σ , ε , t , t' and “,” denote stress, strain, time, Boltzmann integral variable and differential operator, respectively. Also, λ , λ_1 and μ stand for Lamé coefficients that are defined in the viscoelastic domain as (Brinson and Brinson 2008; Zamani 2021a):

$$\begin{aligned} \lambda(z, \omega) &= K(z, \omega) - \frac{2}{3}G(z, \omega) \\ \lambda_1(z, \omega) &= K(z, \omega) + \frac{4}{3}G(z, \omega) \\ \mu(z, \omega) &= G(z, \omega) \end{aligned} \tag{2}$$

where K and G denote bulk and shear moduli, respectively. Moreover, the introduced moduli are related to other constants in the elastic domain as (Brinson and Brinson 2008):

$$\begin{aligned} \lambda &= \frac{\nu E}{(1-2\nu)(1+\nu)} \\ \lambda_1 &= \frac{(1-\nu)}{\nu} \lambda \\ \mu &= \frac{E}{2(1+\nu)} \end{aligned} \tag{3}$$

where ν and E denote the Poisson ratio and Young’s modulus, respectively. It should be noted that the mentioned properties in Eq. (3) could be derived in the viscoelastic domain in terms of time or frequency using the Alfrey correspondence principle (Alfrey 1944). Furthermore, the effective mechanical properties of FGV open-cell foam plates are expressed as (Srinivas and Rao 1971; Hatami et al. 2008; Altenbach and Eremeyev 2008a,b,c; Hosseini-Hashemi et al. 2015; Zamani et al. 2018; Zamani 2021b):

$$\begin{aligned} \rho(z, \omega) &= \rho_s V(z) \\ K(z, \omega) &= K_0 V^2(z) \end{aligned} \tag{4}$$

$$\tag{5}$$

$$G(z, \omega) = G_0 \frac{1 + ic_1\omega}{1 + i\beta c_1\omega} V^2(z), \quad c_1 = h\sqrt{\frac{\rho}{G_0}} \tag{6}$$

$$V(z) = \frac{\rho_p}{\rho_s} + (1 - \frac{\rho_p}{\rho_s})(\frac{1}{2} - \frac{z}{h})^p \tag{7}$$

where $\rho, \rho_s, \rho_p/\rho_s, p, \beta, K_0$ and G_0 denote density, minimum density, minimal relative density, power index, parameter of constitutive relation, elastic dilatation and distortion moduli, respectively. It is worth noting that $\beta = 0.5, 1$ refers to the standard solid and elastic model, respectively. Also, $p = 0, 1, 2$ refer to homogeneous, linear and quadratic distributions of porosity through thickness, respectively.

2.2 Kinematic relations considering thickness stretching

In the present study, the effects of thickness stretching of FGV foam plates are taken into consideration using three different HSNDTs with polynomial, hyperbolic and integral displacement functions. For the first case, HSNDT-Poly is considered as (Thai and Choi 2014):

$$\begin{aligned} u_1(x, y, z, t) &= u(x, y, t) - zw_{b,x} - f(z)w_{s,x} \\ u_2(x, y, z, t) &= v(x, y, t) - zw_{b,y} - f(z)w_{s,y} \\ u_3(x, y, z, t) &= w_b(x, y, t) + w_s(x, y, t) + g(z)w_z(x, y, t) \end{aligned} \tag{8}$$

$$f = -\frac{z}{4} + \frac{5z^3}{3h^2}$$

$$g = 1 - f_{,z}$$

where u, v and w denote displacements in the x, y and z directions, respectively. In addition, w_b, w_s and w_z refer to the bending, shear and thickness-stretching components of transverse displacement, respectively. As can be seen, cubic functions are considered for $f(z)$ and $g(z)$, which are obtained using stress-free edge conditions on the top and bottom surfaces of the plate (Thai and Choi 2014). Although thickness stretching is implemented through the displacement field, the number of unknowns remains at five, which is similar to HSDT of Reddy and FSDT (Reddy 1984). The relevant linear strain-displacement components are expressed as (Thai and Choi 2014):

$$\begin{aligned} \begin{Bmatrix} \varepsilon_x \\ \varepsilon_y \\ \gamma_{xy} \end{Bmatrix} &= \begin{Bmatrix} u_{,x} \\ v_{,y} \\ u_{,y} + v_{,x} \end{Bmatrix} - z \begin{Bmatrix} w_{b,xx} \\ w_{b,yy} \\ 2w_{b,xy} \end{Bmatrix} - f(z) \begin{Bmatrix} w_{s,xx} \\ w_{s,yy} \\ 2w_{s,xy} \end{Bmatrix} \\ \varepsilon_z &= g_{,z}w_z \\ \begin{Bmatrix} \gamma_{yz} \\ \gamma_{xz} \end{Bmatrix} &= g(z) \begin{Bmatrix} (w_s + w_z)_{,y} \\ (w_s + w_z)_{,x} \end{Bmatrix} \end{aligned} \tag{9}$$

where ε_i ($i = x, y, z$) and γ_i ($i = xy, yz, xz$) denote normal and shear strains, respectively. As can be seen, the normal strain in the thickness direction is proportional to the components of displacement in the thickness direction and differentiation of function $g(z)$ with respect to thickness coordinate. For the second case, the same strains and similar inplane displacement fields are considered, while hyperbolic functions are assumed as (Mantari and

Guedes Soares 2013; Belabed et al. 2014):

$$f(z) = \sinh\left(\frac{z}{h}\right) e^{\frac{1}{5h} \cosh\left(\frac{z}{h}\right)} - \frac{z}{h} \left(\cosh\left(\frac{1}{2}\right) + 1/5h \sinh\left(\frac{1}{2}\right)^2 \right) e^{\frac{1}{5h} \cosh\left(\frac{1}{h}\right)}$$

$$g = 1 - f_{,z}$$
(10)

For the last case, hyperbolic shape functions with the integration form of inplane and transverse displacements are assumed as (Zaoui et al. 2019):

$$u_1(x, y, z, t) = u(x, y, t) - zw_{0,x} + \left(\frac{m\pi}{a}\right)^2 f(z) \int \theta(x, y, t) dx$$

$$u_2(x, y, z, t) = v(x, y, t) - zw_{0,y} + \left(\frac{n\pi}{b}\right)^2 f(z) \int \theta(x, y, t) dy$$

$$u_3(x, y, z, t) = w_0(x, y, t) + g(z)\phi_z(x, y, t)$$

$$f = \frac{\pi h}{\pi^4 + h^4} \left(e^{\frac{hz}{\pi}} \left(\pi^2 \sin\left(\frac{\pi z}{h}\right) + h^2 \cos\left(\frac{\pi z}{h}\right) - h^2 \right) \right), \quad g = f_{,z}$$
(11)

where θ and ϕ_z denote rotations of the normal to the midplane. Also, m and n refer to half-waves in the x and y directions, respectively. Like previous theories, the number of unknowns is five, while the shape function of $g(z)$ is different from previous HSNDTs. The linear strain-displacement relations of this theory can be written as (Zaoui et al. 2019):

$$\begin{Bmatrix} \varepsilon_x \\ \varepsilon_y \\ \gamma_{xy} \end{Bmatrix} = \begin{Bmatrix} u_{,x} \\ v_{,y} \\ u_{,y} + v_{,x} \end{Bmatrix} - z \begin{Bmatrix} w_{0,xx} \\ w_{0,yy} \\ 2w_{0,xy} \end{Bmatrix} + f(z) \begin{Bmatrix} \left(\frac{m\pi}{a}\right)^2 \theta \\ \left(\frac{n\pi}{b}\right)^2 \theta \\ -2\theta_{,xy} \end{Bmatrix}$$

$$\varepsilon_z = g_{,z}\phi_z$$

$$\begin{Bmatrix} \gamma_{yz} \\ \gamma_{xz} \end{Bmatrix} = g(z) \begin{Bmatrix} (-\theta + w_z)_{,y} \\ (-\theta + w_z)_{,x} \end{Bmatrix}$$
(12)

As can be seen, the introduced kinematic relations have the same numbers of unknowns and eventually they will result in the same number of governing equations of motion. To complete this section, it is worth mentioning that there are other kinds of integral functions of displacements that are used for dynamic analysis of FG elastic, laminated composites and sandwich plates, see for instance (Allam et al. 2020; Menasria et al. 2020; Bendenia et al. 2020; Tahir et al. 2021a,b; Zaitoun et al. 2021).

3 Governing equations

In this section, the main aim is to derive the governing equations of FGV open-cell foam plates with thickness stretching using three different HSNDTs in the complex domain. First, the procedure of the first introduced HSNDT is thoroughly explained and then the governing equations of motion are extended for other HSNDTs that have different shape functions of $g(z)$ and $f(z)$.

3.1 HSNDT with polynomial function

In order to derive the governing equations of motion, the dynamic version of the Hamilton principle is applied as (Reddy 2004):

$$\int_{t_1}^{t_2} (\delta U - \delta T) dt = 0$$

$$\delta U = \int_A \int_{-h/2}^{h/2} \left(\sigma_{xx}(\omega) \delta \varepsilon_x + \sigma_{yy}(\omega) \delta \varepsilon_y + \sigma_{zz}(\omega) \delta \varepsilon_z + \sigma_{xy}(\omega) \delta \varepsilon_{xy} + \sigma_{yz}(\omega) \delta \varepsilon_{yz} + \sigma_{xz}(\omega) \delta \varepsilon_{xz} \right) dz dA \tag{13}$$

$$\delta T = \int_A \int_{-h/2}^{h/2} \rho(z, \omega) (u_{1,t} \delta u_{1,t} + u_{2,t} \delta u_{2,t} + u_{3,t} \delta u_{3,t}) dz dA$$

$$\delta u_i = 0, (u_i = u, v, w_0, w_b, w_s, w_z, \theta, \phi_z)$$

where $A, t_1, t_2, \delta u_i, \delta U$ and δT denote area, initial time, terminal time, virtual displacement, virtual strain energy and virtual kinematic energy, respectively. By substitution of Eqs. (8) and (9) and Eqs. (1)–(7) in Eqs. (13), plus integration through thickness and integration by parts to derive the virtual displacements, the governing equations of motion can be expressed based on HSNDT-Hyp as:

$$\delta u : \bar{N}_{x,x}(\omega) + \bar{N}_{xy,y}(\omega) = I_0(\omega) u_{,tt} - I_1(\omega) w_{b,xtt} - J_1(\omega) w_{s,xtt} \tag{14}$$

$$\delta v : \bar{N}_{xy,x}(\omega) + \bar{N}_{y,y}(\omega) = I_0(\omega) v_{,tt} - I_1(\omega) w_{b,ytt} - J_1(\omega) w_{s,ytt} \tag{15}$$

$$\delta w_b : \bar{M}_{x,xx}^b(\omega) + 2\bar{M}_{xy,xy}^b(\omega) + \bar{M}_{y,yy}^b(\omega) = I_0(\omega) (w_b + w_s)_{,tt} + J_0(\omega) w_{z,tt} + I_1(\omega) (u_{,x} + v_{,y})_{,tt} - I_2(\omega) \nabla^2 w_{b,tt} - J_2(\omega) \nabla^2 w_{s,tt} \tag{16}$$

$$\delta w_s : \bar{M}_{x,xx}^s(\omega) + 2\bar{M}_{xy,xy}^s(\omega) + \bar{M}_{y,yy}^s(\omega) + \bar{Q}_{xz,x}(\omega) + \bar{Q}_{yz,y}(\omega) = I_0(\omega) (w_b + w_s)_{,tt} + J_0(\omega) w_{z,tt} + J_1(\omega) (u_{,x} + v_{,y})_{,tt} - J_2(\omega) \nabla^2 w_{b,tt} - K_2(\omega) \nabla^2 w_{s,tt} \tag{17}$$

$$\delta w_z : \bar{Q}_{xz,x}(\omega) + \bar{Q}_{yz,y}(\omega) - \bar{R}_z(\omega) = J_0(\omega) (w_b + w_s)_{,tt} + K_0(\omega) w_{z,tt} \tag{18}$$

where $\bar{N}, \bar{M}, \bar{Q}$ and \bar{R} denote the frequency-dependent stress resultants plus I_i, J_i and K_i ($i = 0, 1, 2$) stand for frequency-dependent mass inertia, which are all defined as (Thai and Choi 2014):

$$\left\{ \begin{array}{l} \bar{N}_i(\omega), \bar{M}_i^b(\omega), \bar{M}_i^s(\omega) \\ \bar{Q}_x(\omega), \bar{Q}_y(\omega) \\ \bar{R}_z(\omega) \end{array} \right\} = \int_{-\frac{h}{2}}^{\frac{h}{2}} \left\{ \begin{array}{l} \sigma_i(1, z, f) \\ \sigma_j g \\ \sigma_z g_{,z} \end{array} \right\} dz, \quad \left(\begin{array}{l} i = x, y, xy \\ j = xz, yz \end{array} \right) \tag{19}$$

$$\left\{ \begin{array}{l} I_i(\omega) \\ J_i(\omega) \\ K_k(\omega) \end{array} \right\} = \int_{-\frac{h}{2}}^{\frac{h}{2}} \left\{ \begin{array}{l} \rho z^i \\ \rho(g, f, zf) \\ \rho(g^2, f^2) \end{array} \right\} dz, \quad \left(\begin{array}{l} i = 0, 1, 2 \\ j = 0, 1, 2 \\ k = 0, 2 \end{array} \right)$$

For the introduced variables of the displacement field, the harmonic functions are assumed as (Rao 2004):

$$\begin{aligned}
 u(x, y, t) &= u(x, y)e^{i\omega t} \\
 v(x, y, t) &= v(x, y)e^{i\omega t} \\
 w_b(x, y, t) &= w_b(x, y)e^{i\omega t} \\
 w_s(x, y, t) &= w_s(x, y)e^{i\omega t} \\
 w_z(x, y, t) &= w_z(x, y)e^{i\omega t} \\
 w_0(x, y, t) &= w_0(x, y)e^{i\omega t} \\
 \theta(x, y, t) &= \theta(x, y)e^{i\omega t} \\
 \phi_z(x, y, t) &= \phi_z(x, y)e^{i\omega t}
 \end{aligned}
 \tag{20}$$

Substitution of the harmonic displacement fields and the constitutive relation in the frequency-dependent stress resultants, Eqs. (14)–(18) are rewritten as:

$$\begin{aligned}
 &\hat{A}_{11}u_{,xx} + \hat{A}_{66}v_{,yy} + (\hat{A}_{12} + \hat{A}_{66})v_{,xy} - \hat{B}_{11}w_{b,xxx} - (\hat{B}_{12} + 2\hat{B}_{66})w_{b,xyy} \\
 &- \hat{B}_{11}^s w_{s,xxx} - (\hat{B}_{12}^s + 2\hat{B}_{66}^s)w_{s,xyy} + \hat{X}_{13}w_{z,x} = I_0(\omega)u_{,tt} - I_1(\omega)w_{b,xtt} - J_1(\omega)w_{s,xtt}
 \end{aligned}
 \tag{21}$$

$$\begin{aligned}
 &\hat{A}_{22}v_{,yy} + \hat{A}_{66}v_{,xx} + (\hat{A}_{12} + \hat{A}_{66})u_{,xy} - \hat{B}_{22}w_{b,yyy} - (\hat{B}_{12} + 2\hat{B}_{66})w_{b,xyy} - \hat{B}_{22}^s w_{s,yyy} \\
 &- (\hat{B}_{12}^s + 2\hat{B}_{66}^s)w_{s,xyy} + \hat{X}_{23}w_{z,y} = I_0(\omega)v_{,tt} - I_1(\omega)w_{b,ytt} - J_1(\omega)w_{s,ytt}
 \end{aligned}
 \tag{22}$$

$$\begin{aligned}
 &\hat{B}_{11}u_{,xxx} + (\hat{B}_{12} + 2\hat{B}_{66})(u_{,xyy} + v_{,xxy}) + \hat{B}_{22}v_{,yyy} - \hat{D}_{11}w_{b,xxx} - \hat{D}_{22}w_{b,yyy} \\
 &- 2(\hat{D}_{12} + 2\hat{D}_{66})w_{b,xyy} - \hat{D}_{11}^s w_{s,xxx} - \hat{D}_{22}^s w_{s,yyy} \\
 &- 2(\hat{D}_{12}^s + 2\hat{D}_{66}^s)w_{s,xyy} + \hat{Y}_{13}w_{z,xx} + \hat{Y}_{23}w_{z,yy}
 \end{aligned}
 \tag{23}$$

$$\begin{aligned}
 &= I_0(\omega)(w_b + w_s)_{,tt} + J_0(\omega)w_{z,tt} + I_1(\omega)(u_{,x} + v_{,y})_{,tt} - I_2(\omega)\nabla^2 w_{b,tt} - J_2(\omega)\nabla^2 w_{s,tt} \\
 &\hat{B}_{11}^s u_{,xxx} + (\hat{B}_{12}^s + 2\hat{B}_{66}^s)(u_{,xyy} + v_{,xxy}) + \hat{B}_{22}^s v_{,yyy} - \hat{D}_{11}^s w_{b,xxx} - \hat{D}_{22}^s w_{b,yyy} \\
 &- 2(\hat{D}_{12}^s + 2\hat{D}_{66}^s)w_{b,xyy} - \hat{H}_{11}^s w_{s,xxx} - \hat{H}_{22}^s w_{s,yyy} - 2(\hat{H}_{12}^s + 2\hat{H}_{66}^s)w_{s,xyy} + \hat{A}_{55}^s w_{s,xx} \\
 &+ \hat{A}_{44}^s w_{s,yy} + (\hat{Y}_{13}^s + \hat{A}_{55}^s)w_{z,xx} + (\hat{Y}_{23}^s + \hat{A}_{44}^s)w_{z,yy} = I_0(\omega)(w_b + w_s)_{,tt} + J_0(\omega)w_{z,tt} \\
 &+ J_1(\omega)(u_{,x} + v_{,y})_{,tt} - J_2(\omega)\nabla^2 w_{b,tt} - K_2(\omega)\nabla^2 w_{s,tt}
 \end{aligned}
 \tag{24}$$

$$\begin{aligned}
 &- \hat{X}_{13}u_{,x} - \hat{X}_{23}v_{,y} + \hat{Y}_{13}w_{b,xx} + \hat{Y}_{23}w_{b,yy} + (\hat{Y}_{13}^s + \hat{A}_{55}^s)w_{s,xx} + (\hat{Y}_{23}^s + \hat{A}_{44}^s)w_{s,yy} \\
 &+ \hat{A}_{55}^s w_{z,xx} + \hat{A}_{44}^s w_{z,yy} - \hat{Z}_{33}w_z = J_0(\omega)(w_b + w_s)_{,tt} + K_0(\omega)w_{z,tt}
 \end{aligned}
 \tag{25}$$

where the frequency-dependent coefficients are described as:

$$(\hat{A}_{ij}, \hat{A}_{ij}^s, \hat{B}_{ij}, \hat{B}_{ij}^s, \hat{D}_{ij}, \hat{D}_{ij}^s, \hat{H}_{ij}^s) = \int_{-h/2}^{h/2} \hat{C}_{ij}(\omega, z) (1, g^2, z, f, z^2, fz, f^2) dz$$

$$\begin{aligned}
 (\hat{X}_{ij}, \hat{Y}_{ij}, \hat{Y}_{ij}^s, \hat{Z}_{ij}) &= \int_{-h/2}^{h/2} \hat{C}_{ij}(\omega, z) g_{,z}(1, z, f, g_{,z}) dz \tag{26} \\
 \hat{C}_{ij}(\omega, z) &= \omega \int_0^\infty C_{ij}(\xi, z) e^{-\omega\xi} d\xi
 \end{aligned}$$

where C_{ij} and ξ denote the general form of stiffness coefficient and time variable of the Boltzmann integral, respectively. As mentioned in Eq. (2), the frequency-dependent stiffness coefficients of plates are related to each other as (Brinson and Brinson 2008):

$$\begin{aligned}
 \lambda(\omega, z) + 2\mu(\omega, z) &= \lambda_1(\omega, z) \\
 \hat{C}_{12}(\omega) + 2\hat{C}_{66}(\omega) &= \hat{C}_{11}(\omega) \\
 \hat{C}_{11}(\omega) &= \hat{C}_{22}(\omega) = \hat{C}_{33}(\omega) \tag{27} \\
 \hat{C}_{13}(\omega) &= \hat{C}_{23}(\omega) = \hat{C}_{12}(\omega) \\
 \hat{C}_{44}(\omega) &= \hat{C}_{55}(\omega)
 \end{aligned}$$

These relations can be applied through Eqs. (21)–(25) so that the modified version of the governing equations of motion may be expressed as:

$$\begin{aligned}
 \hat{A}_{11}u_{,xx} + \hat{A}_{66}u_{,yy} + (\hat{A}_{12} + \hat{A}_{66})v_{,xy} - \hat{B}_{11}\nabla^2 w_{b,x} - \hat{B}_{11}^s\nabla^2 w_{s,x} + \hat{X}_{13}w_{z,x} \\
 = I_0(\omega)u_{,tt} - I_1(\omega)w_{b,xtt} - J_1(\omega)w_{s,xtt} \tag{28}
 \end{aligned}$$

$$\begin{aligned}
 \hat{A}_{22}v_{,yy} + \hat{A}_{66}v_{,xx} + (\hat{A}_{12} + \hat{A}_{66})u_{,xy} - \hat{B}_{22}\nabla^2 w_{b,y} - \hat{B}_{22}^s\nabla^2 w_{s,y} + \hat{X}_{23}w_{z,y} \\
 = I_0(\omega)v_{,tt} - I_1(\omega)w_{b,ytt} - J_1(\omega)w_{s,ytt} \tag{29}
 \end{aligned}$$

$$\begin{aligned}
 \hat{B}_{11}\nabla^2 (u_{,x} + v_{,y}) - \hat{D}_{11}\nabla^4 w_b - \hat{D}_{11}^s\nabla^4 w_s + \hat{Y}_{13}\nabla^2 w_{,z} = I_0(\omega) (w_b + w_s)_{,tt} \\
 + J_0(\omega)w_{z,tt} + I_1(\omega) (u_{,x} + v_{,y})_{,tt} - I_2(\omega)\nabla^2 w_{b,tt} - J_2(\omega)\nabla^2 w_{s,tt} \tag{30}
 \end{aligned}$$

$$\begin{aligned}
 \hat{B}_{11}^s\nabla^2 (u_{,x} + v_{,y}) - \hat{D}_{11}^s\nabla^4 w_b - \hat{H}_{11}^s\nabla^4 w_s + \hat{Y}_{13}^s\nabla^2 w_z + \hat{A}_{44}^s\nabla^2 (w_s + w_z) \\
 = I_0(\omega) (w_b + w_s)_{,tt} + J_0(\omega)w_{z,tt} + J_1(\omega) (u_{,x} + v_{,y})_{,tt} - J_2(\omega)\nabla^2 w_{b,tt} - K_2(\omega)\nabla^2 w_{s,tt} \tag{31}
 \end{aligned}$$

$$\begin{aligned}
 -\hat{X}_{13} (u_{,x} + v_{,y}) + \hat{Y}_{13}\nabla^2 (w_b + w_s) + \hat{A}_{44}^s\nabla^2 (w_s + w_z) - \hat{Z}_{33}w_z \\
 = J_0(\omega) (w_b + w_s)_{,tt} + K_0(\omega)w_{z,tt} \tag{32}
 \end{aligned}$$

$$\begin{aligned}
 \nabla^2 () &= ()_{,xx} + ()_{,yy} \\
 \nabla^4 () &= \nabla^2 (\nabla^2 ()) = ()_{,xxxx} + 2 ()_{,xxyy} + ()_{,yyyy} \tag{33}
 \end{aligned}$$

where $\nabla^2 ()$ and $\nabla^4 ()$ are the Nabla and biharmonic operator, respectively.

3.2 HSNDT with hyperbolic functions

For HSNDT with hyperbolic functions of $f(z)$ and $g(z)$, the same computational approach and simplifying relations are used to derive the governing equations so that the final forms of equations are similar to HSNDT with polynomial functions, although different functions of $f(z)$ and $g(z)$ are used (Mantari and Guedes Soares 2013; Belabed et al. 2014).

3.3 HSNDT with integration functions

To derive the governing equations of motion, the same computational approach in conjunction with Eqs. (19) and (20) is used. The five coupled PDEs of motions based on HSNDT with integral (HSNDT-Int) functions (Zaoui et al. 2019) are obtained as:

$$\delta u : \bar{N}_{x,x}(\omega) + \bar{N}_{xy,y}(\omega) = I_0(\omega)u_{,tt} - I_1(\omega)w_{0,xtt} - J_1(\omega)\theta_{,xtt} \tag{34}$$

$$\delta v : \bar{N}_{xy,x}(\omega) + \bar{N}_{y,y}(\omega) = I_0(\omega)v_{,tt} - I_1(\omega)w_{0,ytt} - J_1(\omega)\theta_{,ytt} \tag{35}$$

$$\begin{aligned} \delta w_b : \bar{M}_{x,xx}^b(\omega) + 2\bar{M}_{xy,xy}^b(\omega) + \bar{M}_{y,yy}^b(\omega) &= I_0(\omega)w_{0,tt} + J_0(\omega)\phi_{z,tt} \\ + I_1(\omega)(u_{,x} + v_{,y})_{,tt} - I_2(\omega)\nabla^2 w_{0,tt} - J_2(\omega)\nabla^2 \theta_{,tt} \end{aligned} \tag{36}$$

$$\begin{aligned} \delta \theta : -\left(\frac{m\pi}{a}\right)^2 \bar{M}_x^s(\omega) + \bar{M}_{xy,xy}^s(\omega) - \left(\frac{n\pi}{b}\right)^2 \bar{M}_y^s(\omega) - \bar{Q}_{xz,x}(\omega) \\ - \bar{Q}_{yz,y}(\omega) = J_1(\omega)(u_{,x} + v_{,y})_{,tt} - J_2(\omega)\nabla^2 w_{0,tt} - K_2(\omega)\nabla^2 \theta_{,tt} \end{aligned} \tag{37}$$

$$\delta \phi : \bar{Q}_{xz,x}(\omega) + \bar{Q}_{yz,y}(\omega) - \bar{R}_z(\omega) = J_0(\omega)w_{0,tt} + K_0(\omega)\phi_{z,tt} \tag{38}$$

Where the stress resultant, moment of inertia and coefficients have similar definitions to the previous counterparts. Using the linear strains in Eq. (12), the displacement field in Eq. (11) and the stiffness coefficients in Eq. (26), the governing equations of motion in terms of displacements can be presented as:

$$\begin{aligned} \hat{A}_{11}u_{,xx} + \hat{A}_{66}u_{,yy} + (\hat{A}_{12} + \hat{A}_{66})v_{,xy} - \hat{B}_{11}\nabla^2 w_{0,x} + \left(\left(\frac{m\pi}{a}\right)^2 \hat{B}_{11}^s + \left(\frac{n\pi}{b}\right)^2 \hat{B}_{12}^s\right)\theta_{,x} \\ - 2\hat{B}_{66}^s\theta_{,xyy} + \hat{X}_{13}\phi_{z,x} = I_0(\omega)u_{,tt} - I_1(\omega)w_{0,xtt} - J_1(\omega)\theta_{,xtt} \end{aligned} \tag{39}$$

$$\begin{aligned} \hat{A}_{22}v_{,yy} + \hat{A}_{66}v_{,xx} + (\hat{A}_{12} + \hat{A}_{66})u_{,xy} - \hat{B}_{22}\nabla^2 w_{0,y} + \left(\left(\frac{m\pi}{a}\right)^2 \hat{B}_{12}^s + \left(\frac{n\pi}{b}\right)^2 \hat{B}_{22}^s\right)\theta_{,y} \\ - 2\hat{B}_{66}^s\theta_{,xxy} + \hat{X}_{23}\phi_{z,y} = I_0(\omega)v_{,tt} - I_1(\omega)w_{0,ytt} - J_1(\omega)\theta_{,ytt} \end{aligned} \tag{40}$$

$$\begin{aligned} \hat{B}_{11}\nabla^2(u_{,x} + v_{,y}) - \hat{D}_{11}\nabla^4 w_0 + \left(\left(\frac{m\pi}{a}\right)^2 \hat{D}_{11}^s + \left(\frac{n\pi}{b}\right)^2 \hat{D}_{12}^s\right)\theta_{,xx} \\ + \left(\left(\frac{m\pi}{a}\right)^2 \hat{D}_{12}^s + \left(\frac{n\pi}{b}\right)^2 \hat{D}_{22}^s\right)\theta_{,yy} - 4\hat{D}_{66}^s\theta_{,xxyy} + \hat{Y}_{13}\nabla^2 \phi_z \\ = I_0(\omega)w_{0,tt} + J_0(\omega)\phi_{z,tt} + I_1(\omega)(u_{,x} + v_{,y})_{,tt} - I_2(\omega)\nabla^2 w_{0,tt} - J_2(\omega)\nabla^2 \theta_{,tt} \\ - \left(\left(\frac{m\pi}{a}\right)^2 \hat{B}_{11}^s + \left(\frac{n\pi}{b}\right)^2 \hat{B}_{12}^s\right)u_{,x} - \left(\left(\frac{m\pi}{a}\right)^2 \hat{B}_{12}^s + \left(\frac{n\pi}{b}\right)^2 \hat{B}_{22}^s\right)v_{,y} \\ + 2\hat{B}_{66}^s(u_{,y} + v_{,x})_{,xy} + \left(\left(\frac{m\pi}{a}\right)^2 \hat{D}_{11}^s + \left(\frac{n\pi}{b}\right)^2 \hat{D}_{12}^s\right)w_{0,xx} + \left(\left(\frac{m\pi}{a}\right)^2 \hat{D}_{12}^s + \left(\frac{n\pi}{b}\right)^2 \hat{D}_{22}^s\right)w_{0,yy} \\ - 4\hat{D}_{66}^s w_{0,xyy} - \left(\left\{\left(\frac{m\pi}{a}\right)^2 + \left(\frac{n\pi}{b}\right)^2\right\} \hat{H}_{11}^s + 2\left(\frac{m\pi}{a}\right)\left(\frac{n\pi}{b}\right) \hat{H}_{12}^s\right)\theta + \hat{A}_{55}^s \nabla^2 \theta - 4\hat{H}_{66}^s \theta_{,xxyy} \\ - \left(\left(\frac{m\pi}{a}\right)^2 + \left(\frac{n\pi}{b}\right)^2\right) \hat{Y}_{13} \phi_z - \hat{A}_{55}^s \nabla^2 \phi_z = J_1(\omega)(u_{,x} + v_{,y})_{,tt} - J_2(\omega)\nabla^2 w_{0,tt} \\ - K_2(\omega)\nabla^2 \theta_{,tt} \end{aligned} \tag{41}$$

$$- \hat{X}_{13}(u_{,x} + v_{,y}) + \hat{Y}_{13}\nabla^2 w_0 + \left(\left(\frac{m\pi}{a}\right)^2 + \left(\frac{n\pi}{b}\right)^2\right)(\hat{A}_{44}^s - \hat{Y}_{13})\theta \tag{42}$$

$$+ \hat{A}_{44}^s \nabla^2 \phi_z - \hat{Z}_{33}\phi_z = J_0(\omega)w_{0,tt} + K_0(\omega)\phi_{z,tt} \tag{43}$$

where the definitions of the frequency-dependent coefficients and five unknown elements of displacement are similar to the expressed definitions in Eqs. (26) and (11), respectively. It is

worth noting that the presented equations, (21)–(25), (28)–(33), (34)–(38) and (39)–(43) are derived explicitly in the complex domain for the first time, here.

4 Semianalytical solution

In this section, the introduced equations are solved via a combination of a semianalytical and numerical algorithm to achieve the natural frequencies and modal loss factors of plates under simply supported edge conditions. First, the Galerkin weighed residual method is applied to discretize the five-coupled PDEs of motion in the spatial domain. Suitable shape functions that satisfy movable simply supported edge conditions are written as (Thai and Choi 2014; Belabed et al. 2014; Zaoui et al. 2019):

$$\begin{aligned}
 u(x, y) &= \cos\left(\frac{m\pi}{a}x\right) \sin\left(\frac{n\pi}{b}y\right) \\
 v(x, y) &= \sin\left(\frac{m\pi}{a}x\right) \cos\left(\frac{n\pi}{b}y\right) \\
 w_b(x, y) &= \sin\left(\frac{m\pi}{a}x\right) \sin\left(\frac{n\pi}{b}y\right) \\
 w_s(x, y) &= \sin\left(\frac{m\pi}{a}x\right) \sin\left(\frac{n\pi}{b}y\right) \\
 w_z(x, y) &= \sin\left(\frac{m\pi}{a}x\right) \sin\left(\frac{n\pi}{b}y\right) \\
 w_0(x, y) &= \sin\left(\frac{m\pi}{a}x\right) \sin\left(\frac{n\pi}{b}y\right) \\
 \theta(x, y) &= \sin\left(\frac{m\pi}{a}x\right) \sin\left(\frac{n\pi}{b}y\right) \\
 \phi_z(x, y) &= \sin\left(\frac{m\pi}{a}x\right) \sin\left(\frac{n\pi}{b}y\right)
 \end{aligned} \tag{44}$$

The application of the Galerkin weighted residual method degrades the PDEs of motion to a system of algebraic equations with complex frequency-dependent coefficients. The resultant algebraic equations take a novel form as:

$$(\mathbf{C}(\omega) - \omega^2 \mathbf{M}(\omega)) \mathbf{q} = 0 \tag{45}$$

where \mathbf{C} , \mathbf{M} and \mathbf{q} denote square matrices of the frequency-dependent stiffness, inertia and vector of displacement, respectively. To solve the algebraic equations in the complex domain, the QZ eigenvalue solver (Golub and Van Loan 2013) is used. Eventually, the complex roots are expressed as (Zamani and Aghdam 2016):

$$\begin{aligned}
 \omega &= \omega^{\text{Re}} + i\omega^{\text{Im}} \\
 \omega_{mn} &= \omega^{\text{Re}} \\
 \eta &= \frac{2\omega^{\text{Re}}\omega^{\text{Im}}}{(\omega^{\text{Re}})^2 - (\omega^{\text{Im}})^2}
 \end{aligned} \tag{46}$$

where η and superscripts Re , Im denote the modal loss factor, real part and imaginary parts of the frequencies, respectively.

5 Results and discussion

In this section, the accuracy of the computations is assessed, and the effects of various parameters on frequencies are taken into consideration. First, the results of the present method are compared with other available results for an elastic Al/Al₂O₃ plate (Belabed et al. 2014; Abualnour et al. 2018; Zaoui et al. 2019; Matsunaga 2008; Thai and Kim 2013), a Al/ZrO₂ plate (Thai and Choi 2014; Belabed et al. 2014; Vel and Batra 2004; Neves et al. 2012b; Neves et al. 2012a, 2013; Ferreira et al. 2006) and a viscoelastic laminated composite plate (Alam and Asnani 1986). The influences of geometrical and constitutive parameters on vibrational characteristics are investigated via comprehensive parametric studies. In the following computations, the material and mechanical properties of FGV open-cell foam plates are assumed as: $\rho_p/\rho_s = 0.65$, $\rho_s = 200 \text{ kg/m}^3$, $G_0 = 2 \text{ GPa}$, $K_0 = 2G_0$, $h = 1$, $\beta = 0.5$, $b/a = 1$, $a/h = 10$, $p = 1$, $(m, n) = (1, 1)$.

5.1 Comparative studies

In this section, the first two nondimensional frequency parameters of elastic Al/Al₂O₃ plates are compared with available results in the literature for Quasi-3D by Matsunaga (2008), RHSDT by Thai and Kim (2013), HSNDT-Hyp by Belabed et al. (2014), Quasi-3D with trigonometric functions (Quasi-3D-Tri) by Abualnour et al. (2018), and Quasi-3D with integration functions (Quasi-3D-Int) by Zaoui et al. (2019). For this case, the considered properties and parameters are assumed as (Matsunaga 2008; Thai and Kim 2013; Belabed et al. 2014; Abualnour et al. 2018; Zaoui et al. 2019):

$$\hat{\omega} = \omega h \sqrt{\rho_c/E_c}, a/b = 1, a/h = 2, 5, 10, p = 0, 0.5, 1, 4, 10, (m, n) = (1, 1), (1, 2).$$

Aluminum (Al-metal): $E_m = 70 \text{ GPa}$, $\rho_m = 2702 \text{ kg/m}^3$.

Alumina (Al₂O₃-ceramic): $E_c = 380 \text{ GPa}$, $\rho_m = 3800 \text{ kg/m}^3$, $\nu_c = 0.3$.

The results of this example are given in Table 1. As can be seen, for very thick plates ($a/h = 2$), the present method predicts more values than those obtained by Quasi-3D (Matsunaga 2008), RHSDT (Thai and Kim 2013), HSNDT-Hyp (Belabed et al. 2014), Quasi-3D-Tri (Abualnour et al. 2018) and Quasi-3D-Int (Zaoui et al. 2019). The main reason for this may be that the weighted residual methods generally and the Galerkin method as a special case predict higher values than exact or Navier solutions. Also, among the considered theories in this work, HSNDT-Hyp results in more values than other used theories. For thick plates ($a/h = 5$), the discrepancies of the present methods with other HSNDTs diminish as the power index increases, so that the discrepancies approximately disappear for $p = 10$. However, for moderately thick plates ($a/h = 10$), the results of the present methods show excellent correlation with other HSNDTs, regardless of power index. In other words, the effects of the solution method on natural frequencies of very thick plates come to the fore, while for moderately thick plates, the effects of the solution procedure clearly wane. The same behavior is also observed for the natural frequencies of the second modes.

The next example investigates the fundamental frequency parameters of Al/ZrO₂ plates in comparison with those reported based on the 3-D exact solution (Vel and Batra 2004), Quasi-3D-SSDT (Neves et al. 2012b), Quasi-3D-HYP (Neves et al. 2012a), Quasi-3D-HSDT (Neves et al. 2013), third-order shear deformation theory with meshless method (TSMT-MLM) (Ferreira et al. 2006), refined plate theory (RPT) (Thai and Choi 2014), HSNDT-Poly (Thai and Choi 2014) and HSNDT-Hyp (Belabed et al. 2014), as presented in Table 2. For this comparison, the considered geometry and parameters are assumed as (Vel

Table 1 A comparison of the fundamental frequency parameter $\hat{\omega}$ for Al/Al₂O₃ plates

| Mode (m, n) | a/h | Method | p | | | | |
|-----------------|-------------|---------------------------|--------|--------|--------|--------|--------|
| | | | 0 | 0.5 | 1 | 4 | 10 |
| 1 (1, 1) | 2 | Quasi-3D ^a | 0.9400 | 0.8233 | 0.7477 | 0.5997 | 0.5460 |
| | | RHSDT ^b | 0.9297 | 0.8110 | 0.7356 | 0.5924 | 0.5412 |
| | | HSNDT-Hyp ^c | 0.9414 | 0.8248 | 0.7516 | 0.6056 | 0.5495 |
| | | Present-Poly | 0.9420 | 0.8253 | 0.7520 | 0.6057 | 0.5497 |
| | | Present-Hyp | 0.9691 | 0.8457 | 0.7614 | 0.6117 | 0.5685 |
| | | Present-Int | 0.9474 | 0.8281 | 0.7546 | 0.6094 | 0.5508 |
| | 5 | Quasi-3D ^a | 0.2121 | 0.1819 | 0.1640 | 0.1383 | 0.1306 |
| | | RHSDT ^b | 0.2113 | 0.1807 | 0.1631 | 0.1378 | 0.1301 |
| | | HSNDT-Hyp ^c | 0.2121 | 0.1825 | 0.1659 | 0.1409 | 0.1318 |
| | | Quasi-3D-Tri ^d | 0.2126 | 0.1829 | 0.1663 | 0.1411 | 0.1320 |
| | | Quasi-3D-Int ^e | 0.2126 | 0.1829 | 0.1663 | 0.1411 | 0.1320 |
| | | Present-Poly | 0.2122 | 0.1825 | 0.1659 | 0.1409 | 0.1318 |
| | | Present-Hyp | 0.2143 | 0.1841 | 0.1674 | 0.1440 | 0.1354 |
| | Present-Int | 0.2129 | 0.1829 | 0.1661 | 0.1414 | 0.1321 | |
| | 10 | Quasi-3D ^a | 0.0578 | 0.0492 | 0.0443 | 0.0381 | 0.0364 |
| | | RHSDT ^b | 0.0577 | 0.0490 | 0.0442 | 0.0381 | 0.0364 |
| | | HSNDT-Hyp ^c | 0.0578 | 0.0494 | 0.0449 | 0.0389 | 0.0368 |
| | | Quasi-3D-Tri ^d | 0.0579 | 0.0495 | 0.0450 | 0.0390 | 0.0369 |
| | | Quasi-3D-Int ^e | 0.0579 | 0.0495 | 0.0450 | 0.0390 | 0.0369 |
| | | Present-Poly | 0.0578 | 0.0494 | 0.0449 | 0.0389 | 0.0368 |
| | | Present-Hyp | 0.0579 | 0.0495 | 0.0450 | 0.0391 | 0.0371 |
| Present-Int | 0.0579 | 0.0494 | 0.0449 | 0.0390 | 0.0369 | | |
| 2 (1, 2) | 2 | Quasi-3D ^a | 1.7406 | 1.5425 | 1.4078 | 1.1040 | 0.9847 |
| | | RHSDT ^b | 1.7233 | 1.5192 | 1.3844 | 1.0919 | 0.9807 |
| | | HSNDT-Hyp ^c | 1.7512 | 1.5798 | 1.4164 | 1.1147 | 0.9958 |
| | | Present-Poly | 1.7534 | 1.5514 | 1.4180 | 1.1155 | 0.9969 |
| | | Present-Hyp | 1.8131 | 1.5984 | 1.4620 | 1.1943 | 1.0789 |
| | | Present-Int | 1.7676 | 1.5582 | 1.4238 | 1.1238 | 0.9990 |
| | 5 | Quasi-3D ^a | 0.4658 | 0.4040 | 0.3644 | 0.3000 | 0.2790 |
| | | RHSDT ^b | 0.4623 | 0.3989 | 0.3607 | 0.2980 | 0.2771 |
| | | HSNDT-Hyp ^c | 0.4659 | 0.4041 | 0.3676 | 0.3047 | 0.2811 |
| | | Quasi-3D-Tri ^d | 0.4674 | 0.4052 | 0.3687 | 0.3052 | 0.2817 |
| | | Quasi-3D-Int ^e | 0.4674 | 0.4052 | 0.3687 | 0.3052 | 0.2817 |
| | | Present-Poly | 0.4660 | 0.4042 | 0.3677 | 0.3047 | 0.2811 |
| | | Present-Hyp | 0.4748 | 0.4106 | 0.3738 | 0.3168 | 0.2947 |
| | | Present-Int | 0.4681 | 0.4052 | 0.3685 | 0.3061 | 0.2818 |

Table 1 (Continued)

| Mode (<i>m, n</i>) | <i>a/h</i> | Method | <i>p</i> | | | | |
|----------------------|------------|---------------------------|----------|--------|--------|--------|--------|
| | | | 0 | 0.5 | 1 | 4 | 10 |
| 10 | | Quasi-3D ^a | 0.1381 | 0.1180 | 0.1063 | 0.0905 | 0.0859 |
| | | RHSDT ^b | 0.1376 | 0.1174 | 0.1059 | 0.0903 | 0.0856 |
| | | HSNDT-Hyp ^c | 0.1381 | 0.1184 | 0.1077 | 0.0923 | 0.0868 |
| | | Quasi-3D-Tri ^d | 0.1383 | 0.1186 | 0.1078 | 0.0924 | 0.0868 |
| | | Quasi-3D-Int ^e | 0.1383 | 0.1186 | 0.1078 | 0.0924 | 0.0868 |
| | | Present-Poly | 0.1380 | 0.1184 | 0.1076 | 0.0922 | 0.0867 |
| | | Present-Hyp | 0.1390 | 0.1191 | 0.1083 | 0.0936 | 0.0884 |
| | | Present-Int | 0.1385 | 0.1186 | 0.1078 | 0.0925 | 0.0869 |

^aMatsunaga (2008); ^bThai and Kim (2013); ^cBelabed et al. (2014); ^dAbualnour et al. (2018); ^eZaoui et al. (2019)

and Batra 2004; Neves et al. 2012b; Neves et al. 2012a, 2013; Ferreira et al. 2006; Thai and Choi 2014; Belabed et al. 2014):

$$\bar{\omega} = \omega h \sqrt{\rho_m/E_m}, a/b = 1, a/h = \sqrt{10}, 5, 10, 20, p = 0, 1, 2, 3, 5, (m, n) = (1, 1).$$

Aluminum (Al-metal): $E_m = 70$ GPa, $\rho_m = 2702$ kg/m³.

Zirconia (ZrO₂-ceramic): $E_c = 200$ GPa, $\rho_c = 5700$ kg/m³, $\nu_c = 0.3$.

As can be seen, the present method demonstrates an acceptable correlation with HSNDTs based on the Navier solution. Similar to the previous example, the discrepancies between the present methods and other solutions of moderately thick plates are negligible. Moreover, the maximum correlations refer to the plates with $a/h = 10, p = 0, a/h = 20, p = 1, a/h = 5, p = 2, 5$. In other words, combinations of low thickness ratio with high power index or high thickness ratio with low power index demonstrate significant correlations.

The last comparative example compares the natural frequencies and loss factors of laminated composite plates with those reported by Alam and Asnani (1986) based on complex moduli and layerwise theory, as tabulated in Table 3. The geometrical properties, lamination scheme and complex moduli of carbon fiber-reinforced plastic are considered as (Alam and Asnani 1986):

$$a/h = 150, b/a = 1, [0]_{4T}, E_{11} = 211 \text{ GPa}, E_{22} = 5.3(1 + 0.5i) \text{ GPa},$$

$$G_{23} = 1.3(1 + 0.5i) \text{ GPa}, G_{12} = G_{13} = 2.6(1 + 0.5i) \text{ GPa}, \nu_{12} = 0.25, \rho = 1524 \text{ kg/m}^3$$

As tabulated, the present results display lower frequencies than other theories due to more flexibility or normal deformations in the thickness direction. Although three theories predict different loss factors with infinitesimal differences, the fundamental frequencies are more sensitive to the thickness-stretching effect rather than loss factors.

5.2 Parametric studies

In this subsection, the effects of various parameters such as aspect ratio (b/a), thickness parameter ($H' = h/a$), power index and different HSNDTs on complex frequencies are investigated.

Table 2 A comparison of the fundamental frequency parameter $\bar{\omega}$ for Al/ZrO₂ plates

| Method | $p = 0$ | | $p = 1$ | | | $alh = 5$ | | |
|----------------------------|-------------------|------------|-----------|------------|------------|-----------|---------|---------|
| | $alh = \sqrt{10}$ | $alh = 10$ | $alh = 5$ | $alh = 10$ | $alh = 20$ | $p = 2$ | $p = 3$ | $p = 5$ |
| 3D-Exact ^a | 0.4658 | 0.0578 | 0.2192 | 0.0596 | 0.0153 | 0.2197 | 0.2211 | 0.2225 |
| Quasi-3D-SSDT ^b | - | - | 0.2193 | 0.0596 | 0.0153 | 0.2198 | 0.2212 | 0.2225 |
| Quasi-3D-HYP ^c | - | - | 0.2193 | 0.0596 | 0.0153 | 0.2201 | 0.2216 | 0.2230 |
| Quasi-3D-HSDT ^d | - | - | 0.2193 | - | - | 0.2200 | 0.2215 | 0.2230 |
| TSDT-MLM ^e | - | - | 0.2188 | 0.0592 | 0.0147 | 0.2188 | 0.2202 | 0.2215 |
| RPT-Navier ^f | 0.4623 | 0.0577 | 0.2169 | 0.0592 | 0.0152 | 0.2178 | 0.2193 | 0.2206 |
| HSNDT-Poly ^f | 0.4661 | 0.0578 | 0.2192 | 0.0597 | 0.0153 | 0.2201 | 0.2214 | 0.2225 |
| HSNDT-Hyp ^g | 0.4659 | 0.0578 | 0.2192 | 0.0597 | 0.0153 | 0.2201 | 0.2214 | 0.2225 |
| Present | | | | | | | | |
| HSNDT-Poly | 0.4660 | 0.0578 | 0.2192 | 0.0597 | 0.0153 | 0.2201 | 0.2214 | 0.2224 |
| HSNDT-Hyp | 0.4748 | 0.0579 | 0.2218 | 0.0599 | 0.0153 | 0.2230 | 0.2236 | 0.2221 |
| HSNDT-Int | 0.4681 | 0.0579 | 0.2306 | 0.0624 | 0.0159 | 0.2196 | 0.2217 | 0.2221 |

^aVel and Batra (2004); ^bNeves et al. (2012b); ^cNeves et al. (2012a); ^dNeves et al. (2013); ^eFerreira et al. (2006); ^fThai and Choi (2014); ^gBelabed et al. (2014)

Table 3 The fundamental frequency and loss factor of composite plates

| Method | ω' | η_s |
|------------------------------|-----------|----------|
| Series solution ^a | 0.108 | 0.036 |
| HSNDT-Poly | 0.101 | 0.038 |
| HSNDT-Hyp | 0.101 | 0.037 |
| HSNDT-Int | 0.100 | 0.035 |

^aAlam and Asnani (1986)

For the first case, the fundamental frequencies and loss factors of FGV foam plates with different shear-deformation theories, $p = 1, 2$, and $b/a = 1$ up to 5 are depicted in Fig. 2. As can be observed, both vibrational characteristics show a decrease as aspect ratio increases. In other words, long, moderately thick FGV foam plates demonstrate less stiffness and damping capability. Also, HSNDT-Int presents the maximum values of frequencies and loss factors. Moreover, it is observed that the vibrational characteristics of square plates with HSNDT-Int, HSNDT-Poly and HSNDT-Hyp depict the most sensitivity to the variation of power index, respectively. Indeed, the fundamental frequencies of the mentioned theories demonstrate 41.54%, 26.90% and 25.29% augmentation, respectively, as the power index decreases from 2 to 1. Furthermore, the counterpart variations of fundamental loss factors are 49.13%, 33.90% and 32.25%, respectively.

The next example considers the thickness parameter and its impacts on the first eight frequencies and loss factors of square plates, as demonstrated in Fig. 3. It should be noted that modes of (1, 2), (1, 3), (1,4), (2, 3) and (2, 4) are equal to (2, 1), (3, 1), (4,1), (3, 2) and (4, 2), respectively. In other words, these modes depict the behavior of the 13 natural frequencies and loss factors of square plates. As can be seen, both vibrational characteristics show a reduction as the thickness ratio increases from 2 up to 30. Actually, the first eight frequencies of plates with HSNDT-Poly show 51.96%, 47.57%, 45.53%, 45.17%, 44.30%, 44.29%, 43.83%, and 43.82% reductions, respectively. The counterpart values of modal loss factors depict 51.15%, 46.77%, 44.70%, 44.33%, 43.43%, 43.39%, 42.92%, and 49.27% reduc-

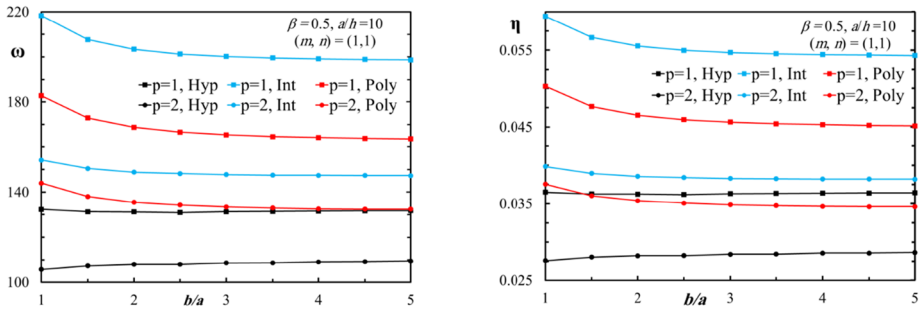


Fig. 2 Fundamental frequencies and loss factors of FGV plates with various power indices and HSNDTs versus aspect ratio

tions, respectively. Moreover, the first eight frequencies of plates with HSNDT-Int display 54.53%, 51.73%, 49.17%, 48.55%, 47.23%, 44.14%, 45.63%, and 44.41% decreases, respectively. The counterpart values of reductions of modal loss factors are 53.17%, 49.03%, 47.41%, 45.99%, 45.78%, 44.86%, 43.90%, and 45.10%, respectively. Furthermore, the first eight frequencies of plates with HSNDT-Hyp depict 56.63%, 58.69%, 56.66%, 56.50%, 54.37%, 53.56%, 50.82%, and 47.79% reductions, respectively. The modal loss factors of plates with HSNDT-Hyp display 52.04%, 58.01%, 55.89%, 55.73%, 52.46%, 51.05%, 48.83%, and 48.84%, reductions, respectively. Based on these values, four remarks can be derived. First, fundamental modes are more sensitive to the thickness parameter rather than other modes, except the (1, 2) and (2, 2) modes of HSNDTs-Hyp. Hence, the thickness parameter plays a crucial role in the design of FGV foam plates that vibrate in their fundamental mode. Secondly, frequencies display more variations than modal loss factors, except the (2, 4) mode of HSNDT-Poly, (1, 4) and the (2, 4) modes of HSNDT-Int, and the (2, 4) mode of HSNDT-Hyp. However, the reduced trends of both vibrational characteristics are not far from each other, regardless of deformation theories. Thirdly, for the constant modes, HSNDT-Hyp demonstrates the most sensitivity to the thickness ratio. Fourthly, as the thickness parameter increases, its impacts on both frequencies and loss factors diminish significantly.

The last example scrutinizes the effects of power indices and HSNDTs on the variation of frequencies and loss factors versus thickness parameter, as demonstrated in Fig. 4. In this example, $p = 1, 2, a/h = 10, b/a = 1$ are assumed. As can be observed, for $p = 1$, the maximum values of frequencies refer to HSNDTs-Int, while the maximum reductions of frequencies are 55.04%, 51.40% and 49.56% for plates with HSNDT-Hyp, HSNDT-Int and HSNDT-Poly, respectively. The relevant reductions of fundamental loss factors are 50.34%, 50.11% and 48.77%, respectively. In other words, the frequency characteristics of FGV foam plates with linear variation of porosity distribution and HSNDT-Hyp show more dependency on variation of the thickness parameter than other deformation theories. However, for $p = 2$ or a quadratic distribution of porosity, a different pattern is observed so that the maximum reductions of fundamental frequencies are 49.19%, 39.45% and 18.37%, which refer to HSNDT-Poly, HSNDT-Int and HSNDT-Hyp, respectively. Furthermore, the maximum reductions of fundamental loss factors are 50.43%, 37.91%, and 36.74% for plates with HSNDT-Poly, HSNDT-Int and HSNDT-Hyp, respectively. Therefore, for the case of a quadratic distribution of porosity, plates with HSNDT-Hyp demonstrate more resistance than other theories against thickness variations, especially fundamental frequencies, which only display a 18.37% reduction.

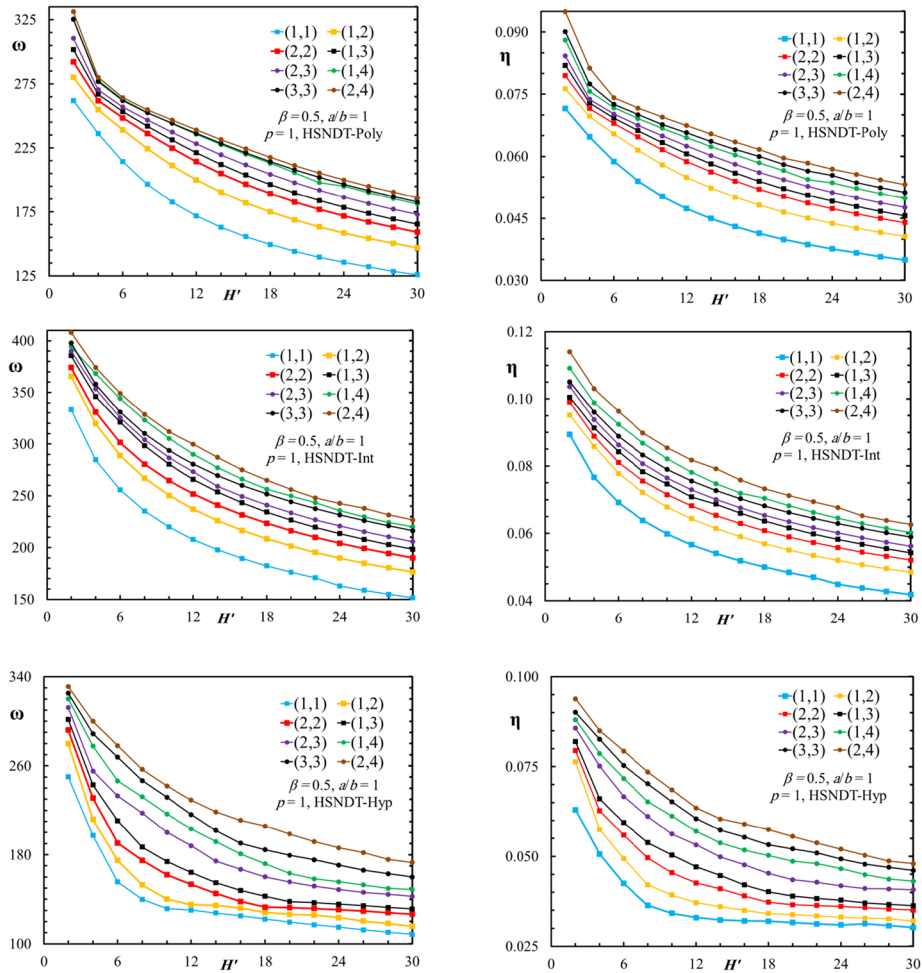


Fig. 3 The first eight frequencies and loss factors of square FGV plates with different theories versus thickness ratio

6 Conclusions

The free-vibration analysis of a functionally graded viscoelastic open-cell foam plate is fulfilled using HSNDTs with polynomial, hyperbolic and integral functions of displacements in order to consider thickness-stretching effects. The Boltzmann superposition principle, a separable kernel framework and a simple power law are applied to achieve constitutive relations, while the Hamilton principle is used to derive the integro-PDEs of motion. The Galerkin method with eigenvalue solver is used to achieve vibrational characteristics. In comparative studies, an acceptable correlation is observed for both FG elastic and viscoelastic composite plates. Through parametric studies, new results are derived and some remarks are presented concisely as:

- HSNDT-Int predicts more values of fundamental frequencies and loss factors than other theories.

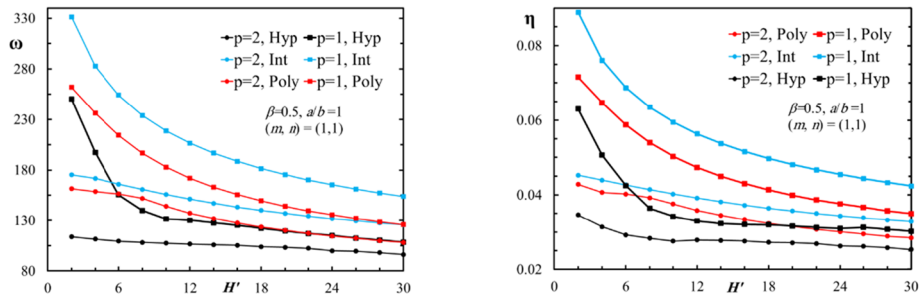


Fig. 4 Fundamental frequencies and loss factors of square FGV plates with various power indices and HSNDTs versus thickness ratio

- By variation of the power index from 1 to 2, the fundamental frequencies of square plates with HSNDT-Int, HSNDT-Poly and HSNDT-Hyp experience 41.54%, 26.90% and 25.29% reduction, while the fundamental loss factors display 49.13%, 33.90% and 32.25% decreases, respectively.
- The fundamental mode is the most affected mode, as the thickness parameter varies. Also, plates with linear variations of porosity and HSNDT-Hyp are more sensitive to the variation of the thickness parameter than other theories.
- For quadratic variations of porosity, HSNDT-Poly and HSNDT-Hyp are the most sensitive and the most resistant to the thickness parameter, respectively; indeed, fundamental frequencies based on polynomial, integral and hyperbolic functions display 49.19%, 37.86% and 18.37% reductions, respectively, while their counterpart loss factors with polynomial, hyperbolic and integral functions demonstrate 44.48%, 36.74%, and 33.12% reductions, respectively.
- The greater the aspect ratio, the less is the stiffness and damping capability of moderately thick FGV foam plates.
- The greater the thickness parameter, the less is its influence on vibrational characteristics.

Funding This research did not receive any specific grant from funding agencies in the public, commercial, or not-for-profit sectors.

Declarations

Conflict of Interest On behalf of all authors, the corresponding author states that there is no conflict of interest.

References

Abualnour, M., Houari, M.S.A., Tounsi, A., Bedia, E.A.A., Mahmoud, S.R.: A novel quasi-3D trigonometric plate theory for free vibration analysis of advanced composite plates. *Compos. Struct.* **184**, 688–697 (2018). <https://doi.org/10.1016/j.compstruct.2017.10.047>

Al Jahwari, F., Huang, Y., Naguib, H.E., Lo, J.: Relation of impact strength to the microstructure of functionally graded porous structures of acrylonitrile butadiene styrene (ABS) foamed by thermally activated microspheres. *Polymer* **98**, 270–281 (2016). <https://doi.org/10.1016/j.polymer.2016.06.045>

Alam, N., Asnani, N.T.: Vibration and damping analysis of fibre reinforced composite material plates. *J. Compos. Mater.* **20**(1), 2–18 (1986). <https://doi.org/10.1177/002199838602000101>

Alfrey, T.: Non-homogeneous stresses in viscoelastic media. *Q. Appl. Math.* **2**(2), 113–119 (1944). <https://doi.org/10.1090/qam/10499>

- Allam, O., Draiche, K., Bousahla, A.A., Bourada, F., Tounsi, A., Benrahou, K.H., Mahmoud, S.R., Bedia, E.A.A., Tounsi, A.: A generalized 4-unknown refined theory for bending and free vibration analysis of laminated composite and sandwich plates and shells. *Comput. Concr.* **26**(2), 185–201 (2020). <https://doi.org/10.12989/cac.2020.26.2.185>
- Altenbach, H., Eremeyev, V.A.: Analysis of the viscoelastic behavior of plates made of functionally graded materials. *J. Appl. Math. Mech.* **88**(5), 332–341 (2008a). <https://doi.org/10.1002/zamm.200800001>
- Altenbach, H., Eremeyev, V.A.: Direct approach-based analysis of plates composed of functionally graded materials. *Arch. Appl. Mech.* **78**(10), 775–794 (2008b). <https://doi.org/10.1007/s00419-007-0192-3>
- Altenbach, H., Eremeyev, V.A.: On the bending of viscoelastic plates made of polymer foams. *Acta Mech.* **204**(3), 137 (2008c). <https://doi.org/10.1007/s00707-008-0053-3>
- Altenbach, H., Eremeyev, V.A.: On the time-dependent behavior of FGM plates. *Key Eng. Mater.* **399**, 63–70 (2009). <https://doi.org/10.4028/www.scientific.net/KEM.399.63>
- Ashby, M.F., Evans, A.G., Fleck, N.A., Gibson, L.J., Hutchinson, J.W., Wadley, H.N.G.: *Metal Foams: A Design Guide*, 1st edn. Butterworth, Woburn (2000)
- Belabed, Z., Ahmed Houari, M.S., Tounsi, A., Mahmoud, S.R., Anwar Bég, O.: An efficient and simple higher order shear and normal deformation theory for functionally graded material (FGM) plates. *Composites, Part B, Eng.* **60**, 274–283 (2014). <https://doi.org/10.1016/j.compositesb.2013.12.057>
- Bendia, N., Zidour, M., Bousahla, A.A., Bourada, F., Tounsi, A., Benrahou, K.H., Bedia, E.A.A., Selim, M.M., Tounsi, A.: Deflections, stresses and free vibration studies of FG-CNT reinforced sandwich plates resting on Pasternak elastic foundation. *Comput. Concr.* **26**(3), 213–226 (2020). <https://doi.org/10.12989/cac.2020.26.3.213>
- Brinson, H.F., Brinson, L.C.: *Polymer Engineering Science and Viscoelasticity an Introduction*, 1st edn. Springer, Boston (2008)
- Carrera, E., Brischetto, S., Cinefra, M., Soave, M.: Effects of thickness stretching in functionally graded plates and shells. *Composites, Part B, Eng.* **42**(2), 123–133 (2011). <https://doi.org/10.1016/j.compositesb.2010.10.005>
- Ferreira, A.J.M., Batra, R.C., Roque, C.M.C., Qian, L.F., Jorge, R.M.N.: Natural frequencies of functionally graded plates by a meshless method. *Compos. Struct.* **75**(1), 593–600 (2006). <https://doi.org/10.1016/j.compstruct.2006.04.018>
- Golub, G.H., Van Loan, C.F.: *Matrix Computations*, 4th edn. Johns Hopkins University Press, Baltimore (2013)
- Gupta, A.K., Kumar, L.: Thermal effect on vibration of non-homogenous visco-elastic rectangular plate of linearly varying thickness. *Meccanica* **43**(1), 47–54 (2008). <https://doi.org/10.1007/s11012-007-9093-3>
- Hatami, S., Ronagh, H.R., Azhari, M.: Exact free vibration analysis of axially moving viscoelastic plates. *Comput. Struct.* **86**(17–18), 1738–1746 (2008). <https://doi.org/10.1016/j.compstruc.2008.02.002>
- Hedayati, R., Sadighi, M.: A micromechanical approach to numerical modeling of yielding of open-cell porous structures under compressive loads. *J. Theor. Appl. Mech.* **54**(3), 769–781 (2016). <https://doi.org/10.15632/jtam-pl.54.3.769>
- Hilton, H.H., Lee, D.H.: Designer functionally graded viscoelastic materials performance tailored to minimize probabilistic failures in panels subjected to aerodynamic noise. *J. Aeroelast. Struct. Dyn.* **2**(3), 1–31 (2012). <http://dx.medra.org/10.3293/asdj.2012.9>
- Hosseini-Hashemi, S., Abaei, A.R., Ilkhani, M.R.: Free vibrations of functionally graded viscoelastic cylindrical panel under various boundary conditions. *Compos. Struct.* **126**, 1–15 (2015). <https://doi.org/10.1016/j.compstruct.2015.02.031>
- Jafari, P., Kiani, Y.: Free vibration of functionally graded graphene platelet reinforced plates: a quasi 3D shear and normal deformable plate model. *Compos. Struct.* **275**, 114409 (2021). <https://doi.org/10.1016/j.compstruct.2021.114409>
- Karamanli, A., Aydogdu, M.: Vibration of functionally graded shear and normal deformable porous microplates via finite element method. *Compos. Struct.* **237**, 111934 (2020). <https://doi.org/10.1016/j.compstruct.2020.111934>
- Mantari, J.L., Guedes Soares, C.: Finite element formulation of a generalized higher order shear deformation theory for advanced composite plates. *Compos. Struct.* **96**, 545–553 (2013). <https://doi.org/10.1016/j.compstruct.2012.08.004>
- Matsunaga, H.: Free vibration and stability of functionally graded plates according to a 2-D higher-order deformation theory. *Compos. Struct.* **82**(4), 499–512 (2008). <https://doi.org/10.1016/j.compstruct.2007.01.030>
- Meksi, A., Benyoucef, S., Houari, M.S.A., Tounsi, A.: A simple shear deformation theory based on neutral surface position for functionally graded plates resting on Pasternak elastic foundations. *Struct. Eng. Mech.* **53**(6), 1215–1240 (2015). <https://doi.org/10.12989/sem.2015.53.6.1215>
- Menasria, A., Kaci, A., Bousahla, A.A., Bourada, F., Tounsi, A., Benrahou, K.H., Tounsi, A., Bedia, E.A.A., Mahmoud, S.R.: A four-unknown refined plate theory for dynamic analysis of FG-sandwich plates under

- various boundary conditions. *Steel Compos. Struct.* **36**(3), 355–367 (2020). <https://doi.org/10.12989/scs.2020.36.3.355>
- Miracle, D.B., Donaldson, S.L., Henry, S.D., Moosbrugger, C., Anton, G.J., Sanders, B.R., Hrivnak, N., Terman, C., Kinson, J., Muldoon, K., Scott, W.W. Jr.: *ASM Handbook, Composites*, vol. 21. ASM International, Materials Park (2001)
- Montgomery, S.M., Hilborn, H., Hamel, C.M., Kuang, X., Long, K.N., Qi, H.J.: The 3D printing and modeling of functionally graded Kelvin foams for controlling crushing performance. *Extreme Mech. Lett.* **46**, 101323 (2021). <https://doi.org/10.1016/j.eml.2021.101323>
- Neves, A.M.A., Ferreira, A.J.M., Carrera, E., Cinefra, M., Roque, C.M.C., Jorge, R.M.N., Soares, C.M.M.: A quasi-3D hyperbolic shear deformation theory for the static and free vibration analysis of functionally graded plates. *Compos. Struct.* **94**(5), 1814–1825 (2012a). <https://doi.org/10.1016/j.compstruct.2011.12.005>
- Neves, A.M.A., Ferreira, A.J.M., Carrera, E., Roque, C.M.C., Cinefra, M., Jorge, R.M.N., Soares, C.M.M.: A quasi-3D sinusoidal shear deformation theory for the static and free vibration analysis of functionally graded plates. *Composites, Part B, Eng.* **43**(2), 711–725 (2012b). <https://doi.org/10.1016/j.compositesb.2011.08.009>
- Neves, A.M.A., Ferreira, A.J.M., Carrera, E., Cinefra, M., Roque, C.M.C., Jorge, R.M.N., Soares, C.M.M.: Static, free vibration and buckling analysis of isotropic and sandwich functionally graded plates using a quasi-3D higher-order shear deformation theory and a meshless technique. *Composites, Part B, Eng.* **44**(1), 657–674 (2013). <https://doi.org/10.1016/j.compositesb.2012.01.089>
- Phung-Van, P., Thai, C.H.: A novel size-dependent nonlocal strain gradient isogeometric model for functionally graded carbon nanotube-reinforced composite nanoplates. *Eng. Comput.* (2021). <https://doi.org/10.1007/s00366-021-01353-3>
- Phung-Van, P., Ferreira, A.J.M., Nguyen-Xuan, H., Thai, C.H.: Scale-dependent nonlocal strain gradient isogeometric analysis of metal foam nanoscale plates with various porosity distributions. *Compos. Struct.* **268**, 113949 (2021). <https://doi.org/10.1016/j.compstruct.2021.113949>
- Rao, S.S.: *Mechanical Vibrations*, 5th edn. Pearson Education, Upper Saddle River (2004)
- Reddy, J.N.: A simple higher-order theory for laminated composite plates. *J. Appl. Mech.* **51**(4), 745–752 (1984). <https://doi.org/10.1115/1.3167719>
- Reddy, J.N.: *Mechanics of Laminated Composite Plates and Shells: Theory and Analysis*, 2nd edn. CRC Press, Boca Raton (2004)
- Sadeghnejad, S., Taraz Jamshidi, Y., Mirzaeifar, R., Sadighi, M.: Modeling, characterization and parametric identification of low velocity impact behavior of time-dependent hyper-viscoelastic sandwich panels. *Proc. Inst. Mech. Eng., Part L, J. Mater. Des. Appl.* **233**(4), 622–636 (2017). <https://doi.org/10.1177/1464420716688233>
- Shariyat, M., Farrokhi, F.: Nonlinear semi-analytical nonlocal strain-gradient dynamic response investigation of phase-transition-induced transversely graded hierarchical viscoelastic nano/micropates. *Proc. Inst. Mech. Eng., Part C, J. Mech. Eng. Sci.* **233**(15), 5388–5409 (2019). <https://doi.org/10.1177/0954406219846145>
- Shariyat, M., Farzan Nasab, F.: Low-velocity impact analysis of the hierarchical viscoelastic FGM plates, using an explicit shear-bending decomposition theory and the new DQ method. *Compos. Struct.* **113**, 63–73 (2014). <https://doi.org/10.1016/j.compstruct.2014.03.003>
- Shariyat, M., Jahangiri, M.: Nonlinear impact and damping investigations of viscoporoelastic functionally graded plates with in-plane diffusion and partial supports. *Compos. Struct.* **245**, 112345 (2020). <https://doi.org/10.1016/j.compstruct.2020.112345>
- Sofiyev, A.H., Zerin, Z., Kuruoglu, N.: Dynamic behavior of FGM viscoelastic plates resting on elastic foundations. *Acta Mech.* (2019). <https://doi.org/10.1007/s00707-019-02502-y>
- Srinivas, S., Rao, A.K.: An exact analysis of free vibrations of simply-supported viscoelastic plates. *J. Sound Vib.* **19**(3), 251–259 (1971). [https://doi.org/10.1016/0022-460X\(71\)90687-0](https://doi.org/10.1016/0022-460X(71)90687-0)
- Tahir, S.I., Chikh, A., Tounsi, A., Al-Osta, M.A., Al-Dulaijan, S.U., Al-Zahrani, M.M.: Wave propagation analysis of a ceramic-metal functionally graded sandwich plate with different porosity distributions in a hygro-thermal environment. *Compos. Struct.* **269**, 114030 (2021a). <https://doi.org/10.1016/j.compstruct.2021.114030>
- Tahir, S.I., Tounsi, A., Chikh, A., Al-Osta, M.A., Al-Dulaijan, S.U., Al-Zahrani, M.M.: An integral four-variable hyperbolic HSDT for the wave propagation investigation of a ceramic-metal FGM plate with various porosity distributions resting on a viscoelastic foundation. *Waves Random Complex Media*, 1–24 (2021b). <https://doi.org/10.1080/17455030.2021.1942310>
- Taraz Jamshidi, Y., Sadeghnejad, S., Sadighi, M.: Viscoelastic behavior determination of EVA elastomeric foams using FEA. In: 23rd Annu. Int. Conf. Mech. Eng.-ISME. Amirkabir University of Technology, Tehran (2015)

- Thai, H.-T., Choi, D.-H.: Improved refined plate theory accounting for effect of thickness stretching in functionally graded plates. *Composites, Part B, Eng.* **56**, 705–716 (2014). <https://doi.org/10.1016/j.compositesb.2013.09.008>
- Thai, H.-T., Kim, S.-E.: A simple higher-order shear deformation theory for bending and free vibration analysis of functionally graded plates. *Compos. Struct.* **96**, 165–173 (2013). <https://doi.org/10.1016/j.compstruct.2012.08.025>
- Thai, C.H., Phung-Van, P.: A meshfree approach using naturally stabilized nodal integration for multilayer FG GPLRC complicated plate structures. *Eng. Anal. Bound. Elem.* **117**, 346–358 (2020). <https://doi.org/10.1016/j.enganabound.2020.04.001>
- Thai, C.H., Ferreira, A.J.M., Carrera, E., Nguyen-Xuan, H.: Isogeometric analysis of laminated composite and sandwich plates using a layerwise deformation theory. *Compos. Struct.* **104**, 196–214 (2013). <https://doi.org/10.1016/j.compstruct.2013.04.002>
- Thai, C.H., Ferreira, A.J.M., Abdel Wahab, M., Nguyen-Xuan, H.: A generalized layerwise higher-order shear deformation theory for laminated composite and sandwich plates based on isogeometric analysis. *Acta Mech* **227**(5), 1225–1250 (2016a). <https://doi.org/10.1007/s00707-015-1547-4>
- Thai, C.H., Zenkour, A.M., Abdel Wahab, M., Nguyen-Xuan, H.: A simple four-unknown shear and normal deformations theory for functionally graded isotropic and sandwich plates based on isogeometric analysis. *Compos. Struct.* **139**, 77–95 (2016b). <https://doi.org/10.1016/j.compstruct.2015.11.066>
- Thai, C.H., Ferreira, A.J.M., Phung-Van, P.: A nonlocal strain gradient isogeometric model for free vibration and bending analyses of functionally graded plates. *Compos. Struct.* **251**, 112634 (2020a). <https://doi.org/10.1016/j.compstruct.2020.112634>
- Thai, C.H., Ferreira, A.J.M., Tran, T.D., Phung-Van, P.: A size-dependent quasi-3D isogeometric model for functionally graded graphene platelet-reinforced composite microplates based on the modified couple stress theory. *Compos. Struct.* **234**, 111695 (2020b). <https://doi.org/10.1016/j.compstruct.2019.111695>
- Vel, S.S., Batra, R.C.: Three-dimensional exact solution for the vibration of functionally graded rectangular plates. *J. Sound Vib.* **272**(3), 703–730 (2004). [https://doi.org/10.1016/S0022-460X\(03\)00412-7](https://doi.org/10.1016/S0022-460X(03)00412-7)
- Zaitoun, M.W., Chikh, A., Tounsi, A., Sharif, A., Al-Osta, M.A., Al-Dulaijan, S.U., Al-Zahrani, M.M.: An efficient computational model for vibration behavior of a functionally graded sandwich plate in a hygrothermal environment with viscoelastic foundation effects. *Eng. Comput.* (2021). <https://doi.org/10.1007/s00366-021-01498-1>
- Zamani, H.A.: Free vibration of doubly-curved generally laminated composite panels with viscoelastic matrix. *Compos. Struct.* **258**, 113311 (2021a). <https://doi.org/10.1016/j.compstruct.2020.113311>
- Zamani, H.A.: Free vibration of viscoelastic foam plates based on single-term Bubnov–Galerkin, least squares, and point collocation methods. *Mech. Time-Depend. Mater.* **25**(3), 495–512 (2021). <https://doi.org/10.1007/s11043-020-09456-y>
- Zamani, H.A., Aghdam, M.M.: Hybrid material and foundation damping of Timoshenko beams. *J. Vib. Control* **23**(18), 2869–2887 (2016). <https://doi.org/10.1177/1077546315624077>
- Zamani, H.A., Aghdam, M.M., Sadighi, M.: Free vibration of thin functionally graded viscoelastic open-cell foam plates on orthotropic visco-Pasternak medium. *Compos. Struct.* **193**, 42–52 (2018). <https://doi.org/10.1016/j.compstruct.2018.03.061>
- Zaoui, F.Z., Ouinas, D., Tounsi, A.: New 2D and quasi-3D shear deformation theories for free vibration of functionally graded plates on elastic foundations. *Composites, Part B, Eng.* **159**, 231–247 (2019). <https://doi.org/10.1016/j.compositesb.2018.09.051>
- Zhang, N.H., Wang, M.L.: A mathematical model of thermoviscoelastic FGM thin plates and Ritz approximate solutions. *Acta Mech.* **181**(3), 153–167 (2006). <https://doi.org/10.1007/s00707-005-0300-9>
- Zhang, N.H., Xing, J.J.: Vibration analysis of linear coupled thermoviscoelastic thin plates by a variational approach. *Int. J. Solids Struct.* **45**(9), 2583–2597 (2008). <https://doi.org/10.1016/j.ijsolstr.2007.12.014>